Contents lists available at ScienceDirect

Journal of Magnetism and Magnetic Materials

journal homepage: http://ees.elsevier.com

Anomalous in-plane coercivity behaviour in hexagonal arrangements of ferromagnetic antidot thin films

M. Salaheldeen[a,b], V. Vega[c], A. Fernández[b], V.M. Prida[b]

[a] Physics Department, Faculty of Science, Sohag University, 82524 Sohag, Egypt
[b] Depto. Física, Universidad de Oviedo, C/ Federico García Lorca 18, 33007 Oviedo, Asturias, Spain
[c] Lab. Membranas Nanoporosas, Servicios Científico-Técnicos, Universidad de Oviedo, Campus El Cristo s/n, 33006 Oviedo, Asturias, Spain

ARTICLE INFO

Keywords
Nanoporous alumina templates
Antidot arrays
Kerr effect
Thin film
Spintronics
Perpendicular magnetic recording

ABSTRACT

An anomalous magnetic behaviour has been observed for transition metal (Fe, Co and Ni) based antidot nanostructures by modifying only the lattice geometry of the nanoholes array. A series of ferromagnetic, FM, antidot arrays have been fabricated by depositing them onto nanoporous alumina membranes with different pore diameters, d, varying in the range between 32 ± 2 and 93 ± 1 nm and maintaining fixed the inter-holes distance, D_{int} = 103 ± 2 nm, and layer thickness, t = 20 nm, but reducing the edge-to-edge separation between adjacent antidots, (W = D_{int} – d). A noticeable change of the in-plane coercivity dependence with W has been observed with an in-plane critical edge to edge distance, $W_{C//}$, at which the in-plane coercivity behaviour with W is changed. In addition, for antidot samples with large W the in-plane hysteresis loops show single-step magnetic behaviour. Meanwhile, the INP hysteresis loops with W < $W_{C//}$ show multistep magnetic behaviour. The decreasing of the in-plane coercivity for FM-antidot samples with W < $W_{C//}$ is correlated with the increase of the out-of-plane contribution to the magnetic anisotropy i.e. increase the out-of-plane coercivity with increasing the nanohole size of antidots. These findings point towards a new nanotechnological strategy of fabrication arrays of magnetic bits, i.e., basic elements for magneto-optic perpendicular recording patterned media, embedded into a continuous 2D structural system and spintronic devices.

1. Introduction

Magnetic antidot arrays are two-dimensional nanostructures that contain an ordered array of periodic lattice of "holes" inserted in a continuous magnetic thin film, which permit them to show unique magnetic properties. The existence of spatially ordered arrays of nanoholes induces a demagnetization field distribution, which can modify the magnetic properties of the continuous thin film such as its magnetization reversal mechanism, the switching field and the intrinsic magnetic anisotropy [1]. In addition, the competition between shape (induced by nanoholes) and intrinsic anisotropy (induced during the film deposition process) makes the antidot arrays intriguing, as the magnetization reversal process is commonly tuned by the lattice parameter of antidot arrays [2], which can behave as pinning centers hindering the displacement of magnetic domain walls [3]. Therefore, the controlled manipulation of nanoholes size and their separation interdistance allows for the possibility to tailor the magnetic hardness of the array [4–6]. Recently, antidot arrays are exciting scientific playgrounds for fundamental research and their application on high density information storage, spintronic, logic circuit and bio magnetic sensing [7–12]. For all these applications, the ability to control the strength and orientation of magnetic anisotropy becomes essential, especially for the thermal stability and switching reliability of magnetic bits. Nevertheless, the astonishing development of nanofabrication techniques in the last decades has opened the door to a new strategy for the patterning of nanostructures, which allows for the modification of the local magnetization distribution in a controlled way [13–17].

In this work, we demonstrate that by properly controlling the geometrical parameters of former alumina templates it can noticeable modify the magnetic properties of ferromagnetic (FM)-antidot arrays thin films. Anomalous in-plane coercivity dependence behaviour with W has been detected for Fe, Co and Ni-antidot arrays samples. Critical in-plane edge-to-edge distances between nanoholes, $W_{C//}$, of 18, 24 and 33 nm have been found for Fe, Co and Ni-antidots, respectively, where the in-plane coercivity starts to decrease with decreasing the W, while the out of plane coercivity increases rapidly with W decreasing. In addition, other critical antidots edge-to-edge distances, $W_{C\perp}$, around of 14 nm and 22 nm have been found for Co and Ni antidots, respectively, where the crossover of the magnetization from the in-plane to out-of-plane occurs.

2. Methodology

The pre-patterned templates for the Fe, Co and Ni-antidots, AD, arrays consisting of hexagonally ordered nanoporous alumina membranes were produced through the conventional two-step mild anodization process [18]. The two-step electrochemical anodization was performed in 0.3 M oxalic acid, at a temperature range between 1 and 3 °C together a potentiostatic applied voltage of 40 V, measured versus a Pt

https://doi.org/10.1016/j.jmmm.2019.165572
Received 19 June 2019; Received in revised form 10 July 2019; Accepted 14 July 2019
Available online xxx

counter electrode. To obtain the highly ordered nanoporous alumina templates, the samples were immersed in 0.2 M CrO_3 and 0.6 M H_3PO_4 aqueous solution. During the second anodization step, which lasted for 5 h, the nanopores grew following the highly self-ordered hexagonal symmetry pre-patterned during the first anodization process. To obtain nanoporous alumina templates with different pore size, the samples were chemically etched in 5 wt% orthophosphoric acid at 30 °C, for different etching times that were varied between 5 and 55 min [19]. This procedure allowed us to obtain a series of nanoporous alumina templates with a wide range of different pore diameter, d, varied between 32 ± 2 and 93 ± 1 nm, but keeping constant their interpore distance, D_{int}, to the fixed value of 103 ± 2 nm. The controlled deposition of the metallic film formed by highly pure metal pieces of high purity FM metals (99.999%), was performed by high vacuum thermal evaporation technique using an E306A thermal vacuum coating unit (Edwards, Crawley, UK) with an ultimate vacuum from 3.8×10^{-7} to 4.3×10^{-7} mbar, having a diffusion pump backed by rotary pumping together with a liquid nitrogen trap [12]. Some pieces of the pure FM transition metal (Fe, Co and Ni) element were placed inside a water-cooled copper crucible and heated under the action of magnetically focused electron ion-beams. The evaporated target metal was deposited on the top-surface of the hexagonally ordered nanoporous alumina membranes, which acted as templates to obtain the ordered arrays of the antidot thin films [20]. Continuous thin films, CTF, were also deposited on a glass substrate, with the same values of thickness than for the antidots samples, in order to compare the obtained results. The experimental details about the deposition conditions have been already reported elsewhere [12,18,19].

After the thermal layer evaporation process, all samples were analyzed using scanning electron microscopy (SEM, JSM 5600, JEOL, Akishima, Tokyo, Japan) to measure the nanohole diameter, d, and the inter-holes distance, D_{int}. Fig. 1(a, b, and c) shows the top view images of selected Co antidot samples with small d, i.e. large W around 73 nm, [Fig. (1a)], and small W around 28 nm and 14 nm, [Fig. (1b)], and [Fig. (1c)]. We observed for all samples a well-ordered hexagonal arrangement of holes with a constant periodicity of 103 ± 2 nm, in good agreement with what is commonly obtained in the patterned alumina substrate after the two-step anodizing procedure in oxalic acid at 40 V.

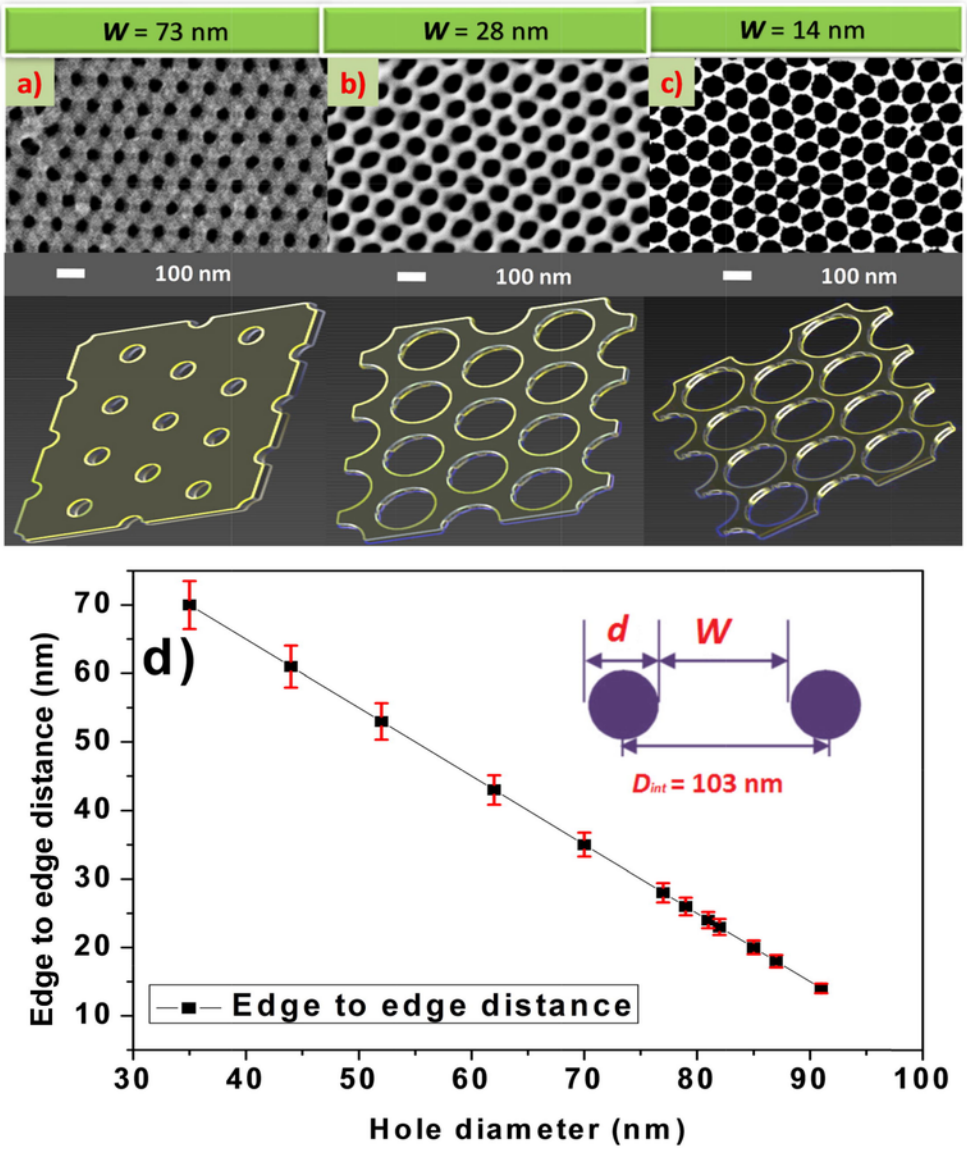

Fig. 1. SEM images of Co layer deposited on the top-surface of nanoporous alumina membranes with varying the antidots edge to edge distance, W: (a) 73 nm, (b) 28 nm and (c) 14 nm. d) edge to edge distance versus hole diameter, d, for Co thin layer deposited on the alumina templates.

Samples with etching time = 53 min show the maximum pore diameter of 93 ± 1 nm, i.e. minimum W ≈ 11 nm, and corresponding hole size around of 89 nm, i.e. W ≈ 14 nm, which can also be achieved for the Fe, Co and Ni-antidot thin film samples, respectively, [Fig. (1c)]. Fig. 1d summarizes the evolution of the antidots edge to edge distance as a function of the hole diameter of Co antidot arrays film. Here, W takes values in the range from 73 nm down to 13 nm, which is plotted as a function of d. A linear relationship is found between W and d as show in [Fig. (1d)]. It is worth to mention that the values for W here reached are lower than the ones previously obtained with similar techniques [21–25].

3. Results and discussion

The surface magneto-optic properties of the Fe, Co and Ni-antidot array thin films were measured making use of a scanning laser Magneto-Optical Kerr Effect (MOKE) magnetometer, NanoMOKE3® (Durham Magneto Optics Ltd., Durham, UK), being able to apply an external magnetic field value up to 0.125 T by using the quadrupole electromagnet option, or up to 0.5 T with the dipole electromagnet option. The NanoMOKE3 magnetometer is matched with p-polarized laser beam and it is sensitive to the longitudinal, transversal and polar- MOKE. The measurements have been done at room temperature (RT) and in both, parallel (In Plane, INP) and perpendicular (Out-of-Plane, OOP) directions to the film plane, respectively.

Fig. 2 represents selected INP and OOP hysteresis loops of Fe, Co and Ni antidot arrays thin films with W ranging between 73 and 14 nm, together with the ones for unpatterned Fe, Co and Ni continuous thin film, CTF, of the same layer thickness with 20 nm, which was employed as a reference sample. Several differences between INP magnetic properties of Fe, Co and Ni antidots have been found comparing to their corresponding CTFs. Firstly; the in-plane hysteresis loops lose its squareness and become wider. This fact is consistent with the scenario where the antidots are acting as pinning centers for the displacement of magnetic domain walls and lead to increasing the in-plane coercivity i.e. wider hysteresis loops [19,26]. Also, the INP loops with W = 18, 22 and 28 nm for Fe, Co and Ni antidot films show multi-step magnetization behaviour, which indicates a strong effect of domain wall pinning and complex magnetization reversal process, as shown in Fig. 2(c, g and k). The possible reason for the multistep magnetic behaviour is attributed to the fact that the material inside the walls of the nanoholes can exhibit a different magnetization orientation, OOP in this case, contributing to the harder magnetic step, while the material in between the pores shows the INP magnetization, corresponding to the softer magnetic step [27–29]. Meanwhile, the hysteresis loops of the small hole diameter, i.e. larger W samples, exhibit a single magnetization reversal step as shown in Fig. 2(b, f and j). For FM-antidot sample with W ≤ 18 nm, a sharp drop of the $H_{C//}$ while increasing in the OOP coercivity, $H_{C\perp}$, have been observed as plotted in Fig. 2(d, h and l), respectively.

Fig. 3 summaries the evolution of $H_{C//}$ and $H_{C\perp}$ of Fe, Co and Ni antidot arrays thin films with respect to W evolution. The maximum value of $H_{C//}$ about 570 Oe was obtained for the Ni antidot sample with W = 33 nm, which is approximately 8.5 times larger than the unpatterned film coercivity. Then, an unexpected $H_{C//}$ decreasing with W appears as indicated in Fig. 3a. The same tendency for $H_{C//}$ has been observed in Fe and Co-antidot arrays with decreasing the edge-to-edge distance, as plotted in Fig. 3a. Maximum $H_{C//}$ values of 1040 Oe with W = 18 nm, and $H_{C//}$ = 765 Oe with W = 24 nm have been found for Fe and Co-antidot samples, respectively. These $H_{C//}$ values are approximately between 15 and 17 times larger than the ones for unpatterned thin film, as shown in Fig. 3(a). Therefore, an in-plane critical edge to edge distance, $W_{C//}$, has been detected for Fe, Co and Ni-antidot samples, where $H_{C//}$ starts to decrease with W decreasing while the out of plane coercivity, $H_{C\perp}$, increase rapidly with W decreasing. Thus, it can be found that the $H_{C//} \alpha 1/W$ for antidot samples above the $W_{C//}$ while the $H_{C//} \alpha W$ for antidot samples below the $W_{C//}$.

A sharp increase in $H_{C\perp}$ for antidot samples with $W < W_{C//}$ has been observed as plotted in Fig. 3. In fact, antidot arrays thin films deposited on the top-surface of nanoporous alumina templates reproduce the intrinsic surface roughness of the patterned templates and develop a crescent shape during the thin film deposition process [28–32]. These two morphological features can determine the magnetic anisotropy of the material. Thus, the magnetic moments between nanoholes remain aligned parallel within the film plane, while magnetic moments along the walls of the nanoholes are perpendicularly aligned to the film plane [19]. The effect on the magnetization component along the perpendicular direction to the sample surface becomes higher and stronger as the W decreases [27,33]. In addition, as W is further decreased, the interdistance between adjacent holes becomes narrower and the film area that has to be nucleated is very small, therefore the magnetization reversal is more favorable via the coherent rotation rather than domain wall movement, which may lead to decrease the $H_{C//}$ [26]. Simultaneously, the $H_{C\perp}$ is increasing rapidly until it reaches the value of $H_{C//}$ at W = 22 nm for Ni antidot and W ≈ 17 nm for Co antidot, as show in Fig. 3a and b.

Therefore, the well-known phenomenological law ($H_{C//} \propto \frac{1}{D_{int}-d} \propto \frac{1}{W}$) [33–41] is found to be not valid for all cases; but it has a limitation corresponding to the current results, where ($H_{C//} \propto \frac{1}{W}$ for $W \geq W_{C//}$ and $H_{C//} \propto W$ for $W < W_{C//}$.

It is worth noting, the relationship between the W of the Fe, Co and Ni antidot array thin films and the coherence radius ($R_{Coh} = \sqrt{24A/\mu_0 M_s^2} = \sqrt{24} l_{ex}$) [42] of (Fe, Co and Ni) since the later refers to the maximum size of a uniformly magnetized particle, where magnetization reversal takes place by coherent rotation rather than domain wall movement [42,43]. Therefore, the reported values of the coherence radius for the magnetic materials within the scope of present study are listed in Table 1.

From comparison between W and R_{Coh} values, it can be found that the $W_{C//} > R_{Coh}$ for Fe, Co, and Ni antidot arrays samples. When R_{Coh} is similar to the value of W, the $H_{C\perp}$ is increasing rapidly until $H_{C\perp} \geq H_{C//}$ for antidot samples with $W \leq R_{Coh}$, as plotted in Fig. 3. Those indicate that for antidot arrays thin film with W close to the R_{Coh} value, where the magnetization reversal mechanism changes from magnetic domain wall movement (for AD with large W) to magnetization rotation of single domain (for AD with short W) [19,26,43,44]. Thus, the crossover of the easy magnetization axis from the INP to OOP direction has been detected at the critical value of the antidots edge-to-edge distance, $W_{C\perp}$, for Ni and Co antidot with $W_{C\perp}$ = 22 nm and 14 nm, respectively. Unfortunately, we could not be able to reach the $W_{C\perp}$ for Fe antidot thin films due the lowest value of W for antidot samples that could be obtained in current work was 14 nm, which is higher than the R_{Coh} of Fe.

4. Conclusion

In summary, the magnetic properties of FM-antidot arrays are strongly dependent on the geometrical parameters of the former nanoporous alumina template. The current results suggest a unified description of the magnetic behaviour of FM-antidot arrays thin films along the change of $H_{C//}$ behaviour with W that takes place at the critical antidots edge-edge distance ($W_{C//}$ = 18 nm, 24 nm and 33 nm) for Fe, Co and Ni-antidot arrays samples, respectively. At the critical edge-edge distance, the maximum $H_{C//}$ has been obtained due to two different complex domain wall pinning mechanism, between the neighbouring holes and inner wall of the holes. The multistep magnetic behaviour observed for antidot samples with $W < W_{C//}$ reveals the strong

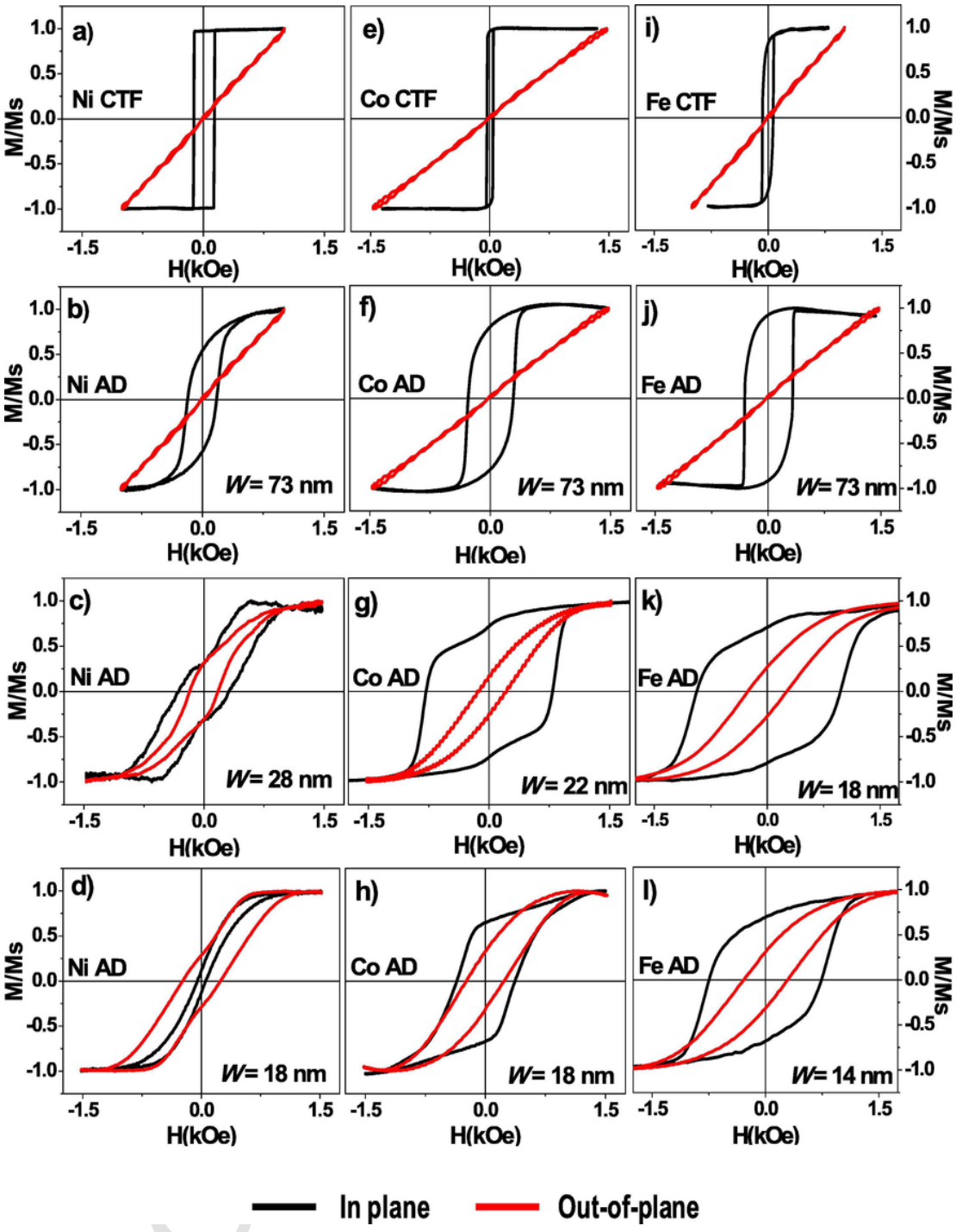

Fig. 2. In-plane (black) and out-of-plane (red) hysteresis loops for antidot arrays with layer thickness of 20 nm; a) Ni CTF, b), c) and d) for Ni AD arrays samples, e) Co CTF, f), g) and h) for Co AD arrays thin film and i) Fe CTF, j), k) and l) for Fe AD arrays films. The antidots edge to edge distance for each sample was specified in the lower right corner of the graphs.

contribution of the OOP component in the magnetization reversal mechanism of the FM-antidots thin films. The magnetization crossover from the INP to OOP directions has been detected for antidot samples with $W_{C\perp} < R_{Coh}$ at 22 nm and 14 nm for Ni and Co antidot arrays samples, respectively. The dual behavior of the INP/OOP coercivity points towards a new nanotechnological strategy of fabrication arrays of magnetic bits, i.e., basic elements for magneto-optic perpendicular recording patterned media, embedded into a continuous 2D structural system.

Acknowledgments

This work has been financially supported under MINECO research project n° MAT2016-76824-C3-3-R. Common Research Services (SCTs) from University of Oviedo are gratefully recognized.

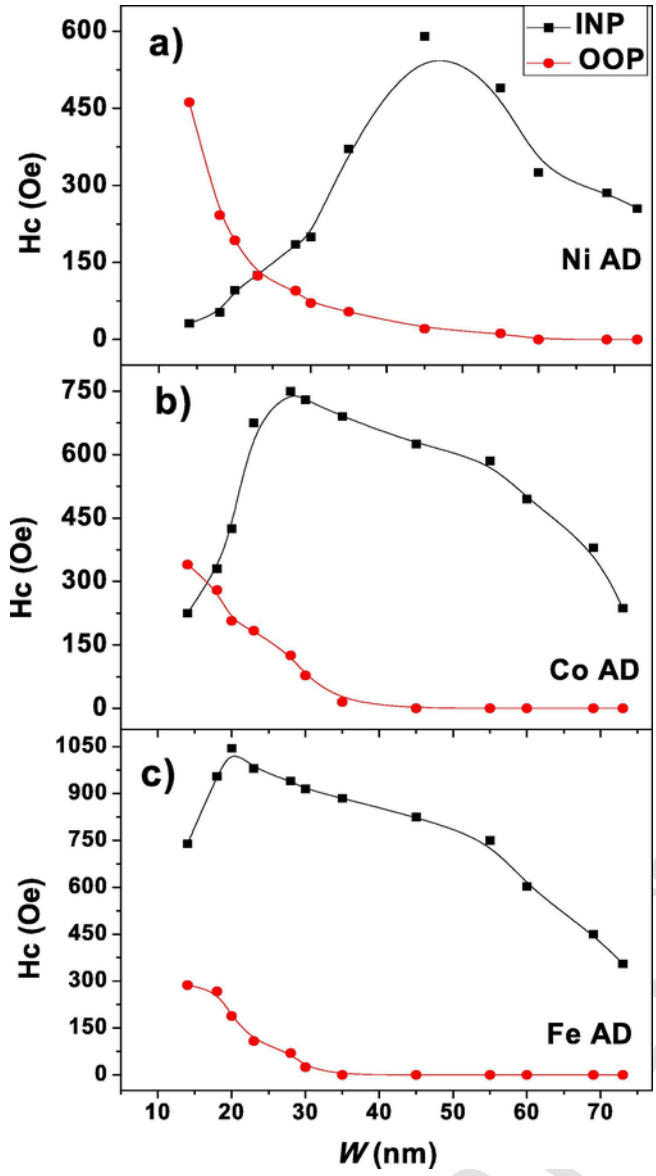

Fig. 3. INP coercivity and OOP coercivity dependence of a) Ni AD, b) Co AD and c) Fe AD thin films with 20 nm layer thickness and different antidots edge-to-edge separation.

Table 1
Room temperature magnetic parameters and coherence radius for ferromagnetic materials and comparing with critical edge to edge distance, W_C.

Materials	l_{ex} (nm)	R_{Coh} (nm)	$W_{C//}$ (nm)	$W_{C\perp}$ (nm)
Fe	2.4 [42]	12 [42]	18	–
Co	3.4 [42]	17 [42]	24	14
Ni	5.1 [42]	25 [42]	33	22

References

[1] R.P. Cowburn, A.O. Adeyeye, J.A.C. Bland, Magnetic domain formation in lithographically defined antidot Permalloy arrays, Appl. Phys. Lett. 70 (1997) 2309, doi:10.1063/1.118845.

[2] Z.L. Xiao, C.Y. Han, U. Welp, H.H. Wang, V.K. Vlasko-Vlasov, W.K. Kwok, D.J. Miller, J.M. Hiller, R.E. Cook, G.A. Willing, G.W. Crabtree, Nickel antidot arrays on anodic alumina substrates, Appl. Phys. Lett. 81 (2002) 2869, doi:10.1063/1.1512993.

[3] C.C. Wang, A.O. Adeyeye, N. Singh, Magnetic antidot nanostructures: effect of lattice geometry, Nanotechnology 17 (2006) 1629, doi:10.1088/0957-4484/17/6/015.

[4] E.T. Papaioannou, V. Kapaklis, P. Patoka, M. Giersig, P. Fumagalli, A. Garcia-Martin, E. Ferreiro-Vila, G. Ctistis, Magneto-optic enhancement and magnetic properties in Fe antidot films with hexagonal symmetry, Phys. Rev. B 81 (5) (2010), doi:10.1103/PhysRevB.81.054424.

[5] P. Vavassori, G. Gubbiotti, G. Zangari, C.T. Yu, H. Yin, H. Jiang, G.J. Mankey, Lattice symmetry and magnetization reversal in micron-size antidot arrays in Permalloy film, J. Appl. Phys. 91 (2002) 7992, doi:10.1063/1.1453321.

[6] M. Jaafar, D. Navas, A. Asenjo, M. Vázquez, M. Hernández-Vélez, J.M. García-Martín, Magnetic domain structure of nanohole arrays in Ni films, J. Appl. Phys. 101 (9) (2007) 09F513, doi:10.1063/1.2711613.

[7] M.T. Rahman, N.N. Shams, C.H. Lai, A large-area mesoporous array of magnetic nanostructure with perpendicular anisotropy integrated on Si wafers, Nanotechnology 19 (2008), doi:10.1088/0957-4484/19/32/325302 325302.

[8] B. Lenk, H. Ulrichs, F. Garbs, M. Münzenberg, The building blocks of magnonics, Phys. Rep. 507 (2011) 107–136, doi:10.1016/j.physrep.2011.06.003.

[9] H. Yu, G. Duerr, R. Huber, M. Bahr, T. Schwarze, F. Brandl, D. Grundler, Omnidirectional spin-wave nanograting coupler, Nat. Commun. 4 (2013) 2702, doi:10.1038/ncomms3702.

[10] J.P. Morgan, A. Stein, S. Langridge, C.H. Marrows, Thermal ground-state ordering and elementary excitations in artificial magnetic square ice, Nat. Phys. 7 (2011) 75–79, doi:10.1038/nphys1853.

[11] P.J. Metaxas, M. Sushruth, R.A. Begley, J. Ding, R.C. Woodward, I.S. Maksymov, M. Albert, W. Wang, H. Fangohr, A.O. Adeyeye, M. Kostylev, Sensing magnetic nanoparticles using nano-confined ferromagnetic resonances in a magnonic crystal, Appl. Phys. Lett. 106 (2015), doi:10.1063/1.4922392 232406.

[12] M. Salaheldeen, V. Vega, A. Ibabe, M. Jaafar, A. Asenjo, A. Fernandez, V.M. Prida, Tailoring of Perpendicular Magnetic Anisotropy in Dy13Fe87 Thin Films with Hexagonal Antidot Lattice Nanostructure, Nanomaterials 8 (2018) 227, doi:10.3390/nano8040227.

[13] R.P.V.D. Xiaoyu Zhang, A.V. Whitney, J. Zhao, E.M. Hicks, Advances in contemporary nanosphere lithographic techniques, J. Nanosci. Nanotechnol. 6 (2006) 1920–1934, doi:10.1166/jnn.2006.322.

[14] J.E.E. Baglin, Ion beam nanoscale fabrication and lithography – a review, Appl. Surf. Sci. 258 (2012) 4103–4111, doi:10.1016/j.apsusc.2011.11.074.

[15] V.R. Manfrinato, L. Zhang, D. Su, H. Duan, R.G. Hobbs, E.A. Stach, K.K. Berggren, Resolution limits of electron-beam lithography toward the atomic scale, Nano Lett. 13 (2013) 1555–1558, doi:10.1021/nl304715p.

[16] J.M.M. Moreno, M. Waleczek, S. Martens, R. Zierold, D. Görlitz, V.V. Martínez, V.M. Prida, K. Nielsch, Constrained order in nanoporous alumina with high aspect ratio: smart combination of interference lithography and hard anodization, Adv. Funct. Mater. 24 (2014) 1857–1863, doi:10.1002/adfm.201303268.

[17] J.M. Shaw, S.E. Russek, T. Thomson, M.J. Donahue, B.D. Terris, O. Hellwig, E. Dobisz, M.L. Schneider, Reversal mechanisms in perpendicularly magnetized nanostructures, Phys. Rev. B – Condens. Matter Mater. Phys. 78 (2008), doi:10.1103/PhysRevB.78.024414 024414.

[18] V.M. Prida, M. Salaheldeen, G. Pfitzer, A. Hidalgo, V. Vega, S. González, J.M. Teixeira, A. Fernández, B. Hernando, Template assisted deposition of ferromagnetic nanostructures: from antidot thin films to multisegmented nanowires, Acta Phys. Pol. A. 131 (2017) 822–827, doi:10.12693/APhysPolA.131.822.

[19] M. Salaheldeen, M. Méndez, V. Vega, A. Fernández, V.M. Prida, Tuning Nanohole Sizes in Ni Hexagonal Antidot Arrays: Large Perpendicular Magnetic Anisotropy for Spintronic Applications, ACS Appl. Nano Mater. 2 (2019) 1866–1875, doi:10.1021/acsanm.8b02205.

[20] R. López Antón, V. Vega, V.M. Prida, A. Fernández, K.R. Pirota, M. Vázquez, Magnetic properties of hexagonally ordered arrays of Fe antidots by vacuum thermal evaporation on nanoporous alumina templates, Solid State Phenom. 152–153 (2009) 273–276 doi: https://doi.org/10.4028/www.scientific.net/SSP.152-153.273.

[21] M.T. Rahman, N.N. Shams, C.H. Lai, J. Fidler, D. Suess, Co/Pt perpendicular antidot arrays with engineered feature size and magnetic properties fabricated on anodic aluminum oxide templates, Phys. Rev. B 81 (1) (2010), doi:10.1103/PhysRevB.81.014418.

[22] K.J. Merazzo, R.P. Del Real, A. Asenjo, M. Vzquez, Dependence of magnetization process on thickness of Permalloy antidot arrays, J. Appl. Phys. 109 (2011) 07B906, doi:10.1063/1.3544483.

[23] F. Béron, A. Kaidatzis, M.F. Velo, L.C.C. Arzuza, E.M. Palmero, R.P. del Real, D. Niarchos, K.R. Pirota, J.M. García-Martín, Nanometer scale hard/soft bilayer magnetic antidots, Nanoscale Res. Lett. 11 (2016) 1–11, doi:10.1186/s11671-016-1302-3.

[24] U. Wiedwald, J. Gräfe, K.M. Lebecki, M. Skripnik, F. Haering, G. Schütz, P. Ziemann, E. Goering, Nowak,, Magnetic switching of nanoscale antidot lattices, Beilstein J. Nanotechnol. 7 (2016) 733–750, doi:10.3762/bjnano.7.65.

[25] D.R. Saldanha, D.A. Dugato, T.J.A. Mori, N.F. Daudt, L.S. Dorneles, J.C. Denardin, Tailoring the magnetic and magneto- transport properties of Pd/Co multilayers and pseudo-spin valve antidots, J. Phys. D. Appl. Phys. 51 (2018), doi:10.1088/1361-6463/aad7ad 395001.

[26] C. Castán-Guerrero, J. Herrero-Albillos, J. Bartolomé, F. Bartolomé, L.A. Rodríguez, C. Magén, F. Kronast, P. Gawronski, O. Chubykalo-Fesenko, K.J. Merazzo, P. Vavassori, P. Strichovanec, J. Sesé, L.M. García, Magnetic antidot to dot crossover in Co and Py nanopatterned thin films, Phys. Rev. B – Condens. Matter Mater. Phys. 89 (2014) 144405, doi:10.1103/PhysRevB.89.144405.

[27] K.J. Merazzo, C. Castán-Guerrero, J. Herrero-Albillos, F. Kronast, F. Bartolomé, J. Bartolomé, J. Sesé, R.P. del Real, L.M. García, M. Vázquez, X-ray photoemission electron microscopy studies of local magnetization in Py antidot array thin films, Phys. Rev. B 85 (18) (2012), doi:10.1103/PhysRevB.85.184427.

[28] Y.H. Jang, J.H. Cho, Morphology-dependent multi-step ferromagnetic reversal processes in Co thin films on crescent-shaped antidot arrays, J. Appl. Phys. 115 (2014), doi:10.1063/1.4864314 063903.

[29] F. Fettar, L. Cagnon, N. Rougemaille, Three-dimensional magnetization profile and multiaxes exchange bias in Co antidot arrays, Appl. Phys. Lett. 97 (2010), doi:10.1063/1.3512864 192502.

[30] T.N.A. Nguyen, J. Fedotova, J. Kasiuk, V. Bayev, O. Kupreeva, S. Lazarouk, D.H. Manh, D.L. Vu, S. Chung, J. Akerman, V. Altynov, A. Maximenko, Effect of flattened surface morphology of anodized aluminum oxide templates on the magnetic properties of nanoporous Co/Pt and Co/Pd thin multilayered films, Appl. Surf. Sci. 427 (2018) 649–655, doi:10.1016/j.apsusc.2017.08.238.

[31] J.P.A.D.C. Leitao, J. Ventura, C.T. Sousa, J.M. Teixeira, J.B. Sousa, M. Jaafar, A. Asenjo, M. Vazquez, J.M. De Teresa, Tailoring the physical properties of thin nanohole arrays grown on flat anodic aluminum oxide templates, Nanotechnology 23 (2012), doi:10.1088/0957-4484/23/42/425701 425701.

[32] F. Béron, K.R. Pirota, V. Vega, V.M. Prida, A. Fernández, B. Hernando, M. Knobel, An effective method to probe local magnetostatic properties in a nanometric FePd antidot array, New J. Phys. 13 (2011), doi:10.1088/1367-2630/13/1/013035 013035.

[33] D. Navas, M. Hernández-Vélez, M. Vázquez, W. Lee, K. Nielsch, Ordered Ni nanohole arrays with engineered geometrical aspects and magnetic anisotropy, Appl. Phys. Lett. 90 (19) (2007) 192501, doi:10.1063/1.2737373.

[34] J. Gräfe, G. Schütz, E.J. Goering, Coercivity scaling in antidot lattices in Fe, Ni, and NiFe thin films, J. Magn. Magn. Mater. 419 (2016) 517–520, doi:10.1016/j.jmmm.2016.06.052.

[35] M. Vázquez, K.R. Pirota, D. Navas, A. Asenjo, M. Hernández-Vélez, P. Prieto, J.M. Sanz, Ordered magnetic nanohole and antidot arrays prepared through replication from anodic alumina templates, J. Magn. Magn. Mater. 320 (2008) 1978–1983, doi:10.1016/j.jmmm.2008.02.053.

[36] E. Paz, F. Cebollada, F.J. Palomares, J.M. González, M.Y. Im, P. Fischer, Scaling of the coercivity with the geometrical parameters in epitaxial Fe antidot arrays, J. Appl. Phys. 111 (2012), doi:10.1063/1.3702584 073908.

[37] I. Ruiz-Feal, L. Lopez-Diaz, A. Hirohata, J. Rothman, C.M. Guertler, J.A.C. Bland, L.M. Garcia, J.M. Torres, J. Bartolome, F. Bartolome, M. Natali, D. Decanini, Y. Chen, Geometric coercivity scaling in magnetic thin film antidot arrays, J. Magn. Magn. Mater. 242–245 (2002) 597–600, doi:10.1016/S0304-8853(01)01108-8.

[38] J.M.T. Bruna, J. Bartolomé, L.M.G. Vinuesa, F.G. Sanchez, J.M. Gonzalez, O.A. Chubykalo-Fesenko, A micromagnetic study of the hysteretic behavior of antidot Fe films, J. Magn. Magn. Mater. 290–291 (2005) 149–152, doi:10.1016/j.jmmm.2004.11.169.

[39] P. Prieto, K.R. Pirota, M. Vazquez, J.M. Sanz, Fabrication and magnetic characterization of permalloy antidot arrays, Phys. Status Solidi Appl. Mater. Sci. 205 (2008) 363–367, doi:10.1002/pssa.200723280.

[40] C. Castán-Guerrero, J. Sesé, J. Bartolomé, F. Bartolomé, J. Herrero-Albillos, F. Kronast, P. Strichovanec, K.J. Merazzo, M. Vázquez, P. Vavassori, L.M. García, Fabrication and Magnetic Characterization of Cobalt Antidot Arrays: Effect of the Surrounding Continuous Film, J. Nanosci. Nanotechnol. 12 (2012) 7437–7441, doi:10.1166/jnn.2012.6537.

[41] C. Castán-Guerrero, J. Bartolomé, F. Bartolomé, L.M. García, J. Sesé, P. Strichovanec, J. Herrero-Albillos, K.J. Merazzo, M. Vázquez, P. Vavassori, Coercivity dependence on periodicity of Co and Py antidot arrays, J. Korean Phys. Soc. 62 (2013) 1521–1524, doi:10.3938/jkps.62.1521.

[42] J.M.D. Coey, Magnetism and Magnetic Materials, Cambridge University Press, 2010, doi:10.1017/CBO9780511845000.

[43] G.S. Abo, Y.K. Hong, J. Park, J. Lee, W. Lee, B.C. Choi, Definition of magnetic exchange length, IEEE Trans. Magn. 49 (2013) 4937–4939, doi:10.1109/TMAG.2013.2258028.

[44] M. Krupinski, D. Mitin, A. Zarzycki, A. Szkudlarek, M. Giersig, M. Albrecht, M. Marszałek, Magnetic transition from dot to antidot regime in large area Co/Pd nanopatterned arrays with perpendicular magnetization, Nanotechnology. 28 (2017), doi:10.1088/1361-6528/aa5656 085302.